Stem Cell Reports
Report
OPEN ACCESS

Epidermal Growth Factor Treatment of the Adult Brain Subventricular Zone Leads to Focal Microglia/Macrophage Accumulation and Angiogenesis

Olle R. Lindberg,[1] Anke Brederlau,[1] and H. Georg Kuhn[1,*]
[1]Center for Brain Repair and Rehabilitation, Institute of Neuroscience and Physiology, Sahlgrenska Academy, University of Gothenburg, Gothenburg 413 90, Sweden
*Correspondence: georg.kuhn@neuro.gu.se
http://dx.doi.org/10.1016/j.stemcr.2014.02.003

SUMMARY

One of the major components of the subventricular zone (SVZ) neurogenic niche is the specialized vasculature. The SVZ vasculature is thought to be important in regulating progenitor cell proliferation and migration. Epidermal growth factor (EGF) is a mitogen with a wide range of effects. When stem and progenitor cells in the rat SVZ are treated with EGF, using intracerebroventricular infusion, dysplastic polyps are formed. Upon extended infusion, blood vessels are recruited into the polyps. In the current study we demonstrate how polyps develop through distinct stages leading up to angiogenesis. As polyps progress, microglia/macrophages accumulate in the polyp core concurrent with increasing cell death. Both microglia/macrophage accumulation and cell death peak during angiogenesis and subsequently decline following polyp vascularization. This model of inducible angiogenesis in the SVZ neurogenic niche suggests involvement of microglia/macrophages in acquired angiogenesis and can be used in detail to study angiogenesis in the adult brain.

INTRODUCTION

The subventricular zone (SVZ) of the lateral ventricle walls is one of the main germinal zones in the adult mammalian brain (Altman, 1969). Adult neurogenesis within the SVZ proceeds via a well-defined sequence of events. Slowly dividing stem cells, so-called B cells, give rise to rapidly proliferating transient amplifying C-cells. Neuroblasts are generated from these proliferating progenitors and migrate to the olfactory bulb, where they differentiate into interneurons (Luskin, 1993; Doetsch et al., 1997).

The environment provided by the cells in the SVZ is very different from that of the surrounding nonneurogenic regions. The unique proneurogenic conditions in the SVZ make up what is called the neurogenic niche (Mirzadeh et al., 2008; Shen et al., 2008; Tavazoie et al., 2008). A specialized vasculature with reduced pericyte coverage is an integral part of the SVZ neurogenic niche (Tavazoie et al., 2008). When stem cells in the SVZ transition from the quiescent B cell stage to the proliferative C-cell stage, they move from a position close to the ependymal cell layer to the underlying vasculature (Kokovay et al., 2010). As the C-cells develop into migratory neuroblasts (A-cells), the vasculature in the SVZ and the rostral migratory stream (RMS) is used as a migratory scaffold, guiding the cells toward the olfactory bulbs (Bovetti et al., 2007). These studies suggest an intimate relationship between SVZ stem and progenitor cells and the specialized vasculature; however, whether the stem and progenitor cells can directly influence the surrounding vasculature is less clear.

We and others have previously studied the effects of intracerebroventricular (ICV) epidermal growth factor (EGF) infusion on neural stem and progenitor cells in the SVZ. Apart from inducing proliferation, EGF infusion reduces the number of neuroblasts, induces atypical migration of oligodendrocyte-like progenitors, stimulates expansion and migration of OLIG2-expressing progenitors in the rostral migratory stream, and leads to polyp formation in the rat SVZ (Craig et al., 1996; Kuhn et al., 1997; Doetsch et al., 2002; Gonzalez-Perez et al., 2009; Lindberg et al., 2012a, 2012b).

Microglia are the resident immune cells of the brain, derived from yolk-sac macrophages. Microglia precursors invade the brain during development before vascularization occurs (Arnold and Betsholtz, 2013). In addition to functions in the immune response and tissue homeostasis, microglia modulate SVZ adult neurogenesis (Walton et al., 2006; Liao et al., 2008). In the retina, microglia are implicated in vascular development, angiogenesis, and capillary sprouting (Checchin et al., 2006; Unoki et al., 2010; Bourghardt Peebo et al., 2011).

We introduce a reproducible model of inducing angiogenesis in the adult SVZ by extended ICV infusion of EGF. Within 14 days of infusion, EGF-induced SVZ polyps attract blood vessels, a process that is preceded by microglia/macrophages accumulation and cell death. The current study suggests an important role of microglia/macrophages in the induction of brain angiogenesis and provides a model by which the early stages of angiogenesis can be readily explored.

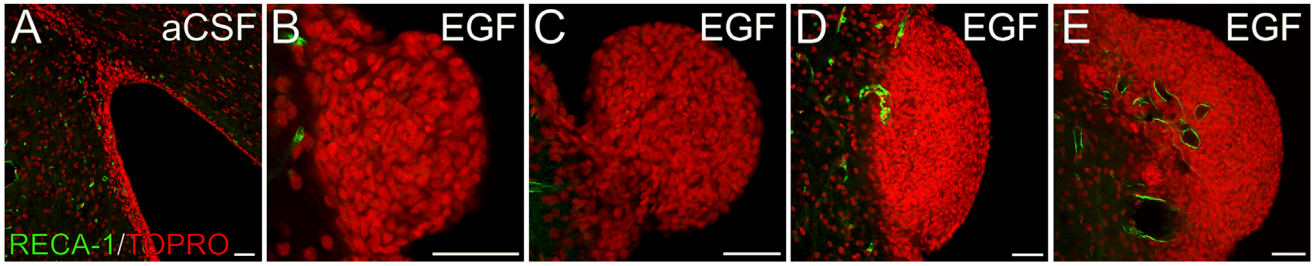

Figure 1. EGF Infusion Induces Polyp Formation and Polyp-Associated Angiogenesis
(A–E) Endothelial cells visualized by RECA-1 (green) and nuclei labeled using TOPRO3 (red) in the vehicle-treated control SVZ (aCSF) (A) and in EGF-induced polyps SVZ (B–D). Polyps formed after 7 days of EGF infusion were present as convex protrusions from the SVZ (B) or as slightly larger spherical structures (C). Following 14 days of EGF infusion polyps were larger and persistently displayed blood vessel recruitment (D) or a complex vascular network in the polyp core (E). Scale bars, 50 μm.

RESULTS

Development of Epidermal-Growth-Factor-Induced Polyp Formation Results in Angiogenesis

We have previously described how ICV infusion of EGF increases proliferation and size of the rat subventricular zone. Prolonged infusion for 14 days induces the formation of focal dysplastic polyps (Kuhn et al., 1997; Lindberg et al., 2012a). The EGF-induced polyps show distinct expression of neural stem cell and progenitor markers and display unique ultrastructural characteristics. In the current study, EGF or artificial cerebrospinal fluid (aCSF) was continuously infused ICV for 7 and 14 days to progressively study polyp formation. No polyps were found in any of the groups receiving aCSF only (Figure 1A). Polyp formation was present in all animals receiving EGF infusion. An average of 1.9 ± 0.5 polyps per 40 μm section (n = 4, mean ± SE) was found in the lateral ventricles following 14 days of EGF infusion. Studying polyps after 7 and 14 days of EGF infusion revealed distinct differences in polyp appearance. Overall, polyps formed over 14 days of EGF infusion were almost three times larger compared to polyps formed over 7 days (22,120 ± 9,366 μm^2 and 63,702 ± 15,094 μm^2, respectively, n = 4 for both groups, p = 0.0034, mean ± SE). A subset of polyps formed convex protrusions from the SVZ showing a relatively small polyp diameter (~50 μm) (Figure 1B). Other polyps were of a spherical shape, occasionally only connected to the SVZ via a small "stem" (Figure 1C). Polyps formed after 14 days of EGF infusion were not only larger, but persistently contained blood vessels. Some polyps had a single vessel leading into the core of the polyp (Figure 1D), whereas others had extensive vascularization in the polyp core (Figure 1E). The polyp blood vessels were more heterogeneous with respect to vessel diameter and morphology than were blood vessels of the control SVZ (Figure 1E).

Changes in Microglia/Macrophages and Angiogenesis Mark Distinct Stages in Polyp Progression

Because of the methodological difficulties in separating microglia from peripherally recruited macrophages, we will make no such distinction and use the term microglia/macrophage or refer to the antigen used to label said population of cells. We used an antibody against IBA1 to label microglia/macrophages and in smaller polyps, we observed $IBA1^+$ cells scattered throughout the polyps at a density similar to the underlying SVZ (Figure 2A). In other polyps the distribution of $IBA1^+$ cells was less random, with a tendency toward accumulating in the core (Figure 2B). The morphology of $IBA1^+$ cells was of a more activated phenotype with shorter and thicker cellular processes compared to $IBA1^+$ cells in smaller polyps (Figure 2B). In animals receiving 14 days of EGF infusion, we found polyps with significant accumulation of $IBA1^+$ cells, occasionally with a single vessel leading into the polyp core (Figure 2C). The majority of $IBA1^+$ cells in the polyp core had a spherical cell body indicative of amoeboid microglia/macrophages (Figure 2C). In highly vascularized polyps, $IBA1^+$ cells were predominantly located in close association with blood vessels, displaying a more ramified appearance compared to amoeboid $IBA1^+$ cells in nonvascularized polyps (Figure 2D). Combining polyp appearance, vascularization, and $IBA1^+$ cell morphology, distinct stages in polyp development became apparent. To facilitate analysis of polyp growth and vascularization, we defined four stages in polyp development (I–IV). At stage I, polyps are beginning to protrude into the ventricular space (Figure 1B), containing $IBA1^+$ cells with a ramified morphology (Figure 2A). At stage II, the polyps take on a spherical shape (Figure 1C) and certain compartmentalization of $IBA1^+$ cells is present (Figure 2B). Early signs of $IBA1^+$ cell core accumulation are present and the $IBA1^+$ cell morphology is more activated, with a round shape and shorter processes (Figure 2B). Seven days of EGF infusion results only in polyps of stages I and II. Following

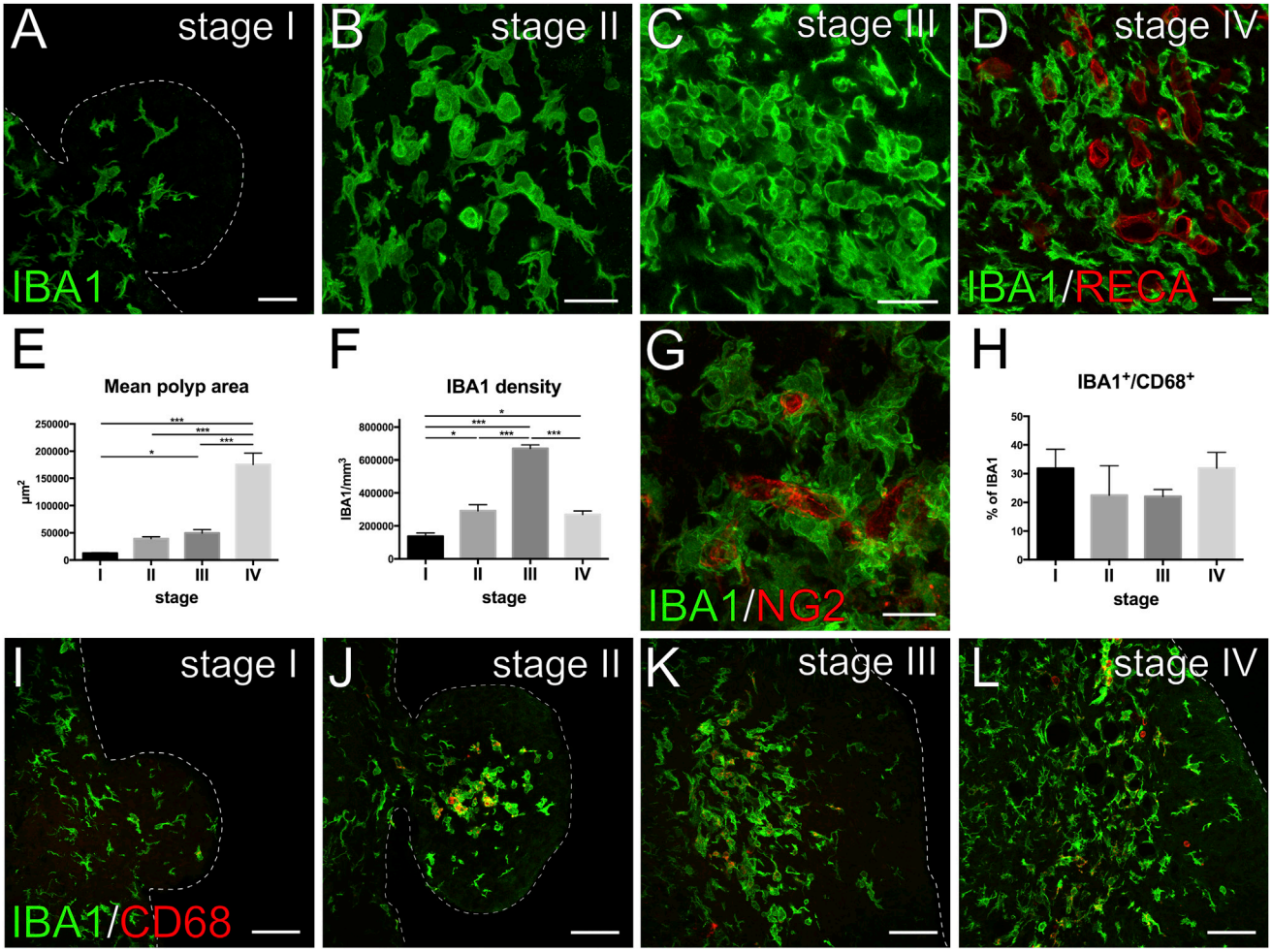

Figure 2. IBA1$^+$ Cell Accumulation, Distribution, and Activation in EGF-Induced Polyps

(A) Microglia/macrophages (IBA1) in small polyps are ramified in appearance with numerous long processes (stage I).

(B) In spherical, slightly larger polyps IBA1$^+$ cells adopt a more reactive morphology with a rounded shape and short processes (stage II).

(C) Polyp with extensive IBA1$^+$ cell accumulation and aggregation of amoeboid IBA1$^+$ cells in the polyp core (stage III).

(D) IBA1$^+$ cells of vascularized polyps are predominately not amoeboid and frequently line blood vessels (RECA, in red) (stage IV).

(E) Mean cross-sectional area of polyps stages I–IV ($F [3, 20] = 58.47$, $p < 0.0001$).

(F) Density of IBA1-labeled IBA1$^+$ cells in polyps stages I–IV ($F [3, 17] = 54.90$, $p < 0.0001$).

(G) IBA1$^+$ cells forming a cage-like structure around angiogenic vessel sprouts. Activated pericytes in angiogenic vessel labeled using NG2.

(H) Percentage of IBA1$^+$ cells coexpressing marker of activation CD68 in polyps stages I–IV ($F [3, 12] = 0.6653$, $p = 0.5893$).

(I–L) Representative images of IBA1 and CD68 expression in polyps stages I–IV.

Scale bars, 25 µm (A–D), 15 µm (G), and 50 µm (I–L). In (E), n(I) = 8, n(II) = 6, n(III) = 5, n(IV) = 5. In (F), n(I) = 5, n(II) = 7, n(III) = 3, n(IV) = 6. In (H), n(I) = 4, n(II) = 3, n(III) = 3, n(IV) = 6. All data are presented as mean ± SEM. *$p < 0.05$; ***$p < 0.001$.

seven additional days of EGF infusion, the first signs of angiogenesis (Figure 1D) and extensive IBA1$^+$ cell core accumulation (Figure 2C) define stage III polyps. The final stage (IV) is characterized by dense polyp core vascularization (Figure 1E) and vessel-associated IBA1$^+$ cells (Figure 2D).

Infusion of EGFR (EGF receptor) ligand TGFα (transforming growth factor alpha) has previously been reported to increase the number of microglia in the SVZ. The TGFα-induced microglia were almost exclusively bromodeoxyuridine (BrdU) negative, suggesting recruitment of microglia to the EGFR-stimulated SVZ (de Chevigny et al., 2008). We injected BrdU three times during the last 24 hr and analyzed the extent of microglial/macrophage proliferation in polyps using IBA1 as a microglia/macrophage marker. Only 2.2% of IBA1$^+$ cells (7/324 cells in five animals) were displaying BrdU immunoreactivity, indicating migration of IBA1$^+$ cells into the EGF-stimulated, hyperproliferative SVZ, rather than local proliferation.

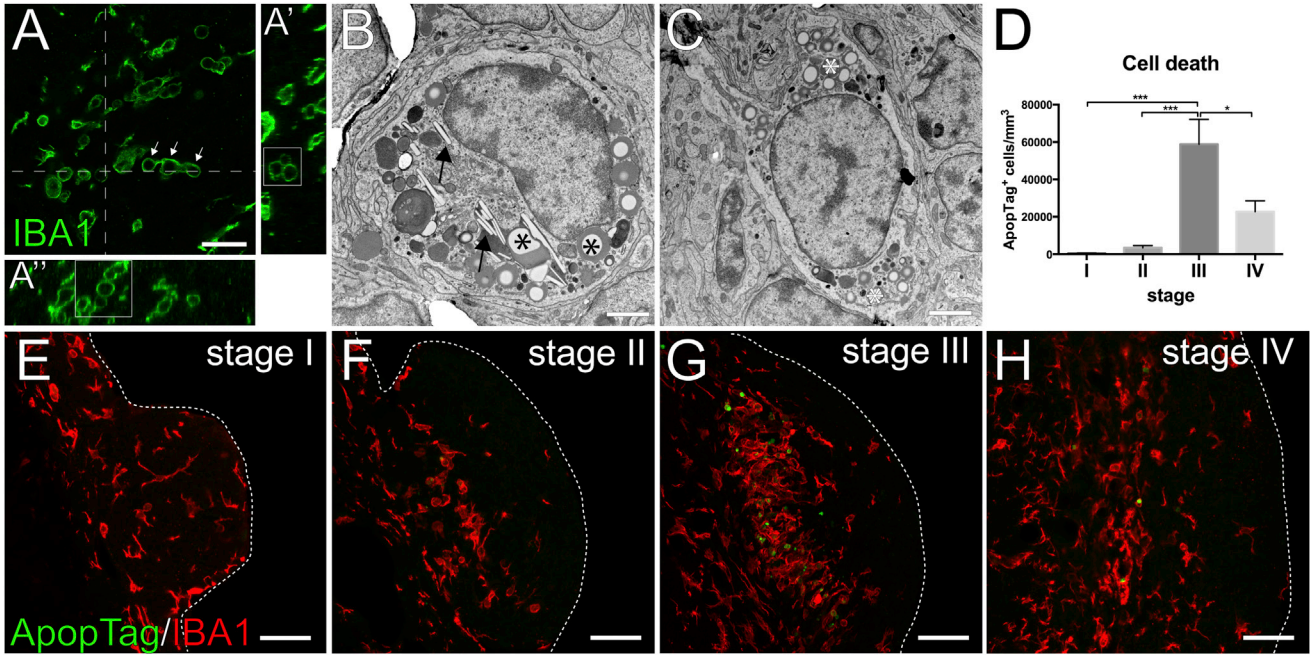

Figure 3. Morphological and Ultrastructural Features of Polyp Microglia/Macrophages and Polyp-Associated Cell Death

(A) IBA1$^+$ cells in angiogenic polyps displaying tight cell-cell association and "string of pearl" structure (arrows) (A). yz axis (A′) and yx (A′′) projection of confocal image stack acquired in (A), showing IBA1$^+$-labeled microglia/macrophage clusters (boxes).

(B) Transmission electron microscopy micrograph of amoeboid cell with intracellular vesicles (*) and cholesterol crystals (arrows) in polyp.

(C) Cell with an abundance of intracellular vesicles (*).

(D) Density of ApopTag-labeled cells in polyps stages I–IV ($F [3, 20] = 15,31$, $p < 0.0001$).

(E–H) Representative images of ApopTag (green) and IBA1 (red) in polyps stages I–IV.

Scale bars, 20 μm (A), 2 μm (B and C), and 50 μm (E–H). In (D), n(I) = 5, n(II) = 9, n(III) = 6, n(IV) = 4. All data are presented as mean ± SEM. *$p < 0.05$; ***$p < 0.001$.

Angiogenesis in Polyps Is Preceded by Microglia/Macrophage Accumulation

Using the established criteria for polyps staging, we measured the average cross-sectional area of the polyps at stages I–IV (Figure 2E). The average area of polyps increased according to stage designation, with stage III polyps showing a larger cross-sectional area compared to stage I, and stage IV polyps having the largest cross-sectional area compared to all other stages (Figure 2E).

Moreover, from stage I to III the density of IBA1$^+$ cells increased substantially, being 3-fold higher in stage III polyps compared to stage I polyps. At stage IV, the density decreased to one-third compared to stage III, a level comparable to stage II (Figure 2F). In stage III polyps, IBA1$^+$ cells were frequently found tightly associated to vessel sprouts. The IBA1$^+$ cells aggregated in cage-like structures around the angiogenic vessels, which were covered by strongly NG2 immunoreactive-activated pericytes (Figure 2G).

Microglia activation is a multistep process based on functional, morphological, and antigenic features (Kettenmann et al., 2011). CD68 is a lipoprotein used as a marker for late-stage microglial activation. IBA1$^+$/CD68$^+$ cells were found in polyps at all stages (Figures 2I–2L). No significant differences were found between any of the stages. The average percentage of CD68-expressing IBA1$^+$ cells was between 20%–30% in all groups (Figure 2H).

Unique Morphological and Ultrastructural Features of Polyp-Associated Microglia/Macrophages

The increasing accumulation of microglia/macrophages in the polyp stages, leading to angiogenesis in stage III, suggests an involvement of microglia/macrophages in the angiogenic process. By acquiring high-density confocal z stacks of IBA1-labeled cells, we were able to distinguish additional morphological features of microglia/macrophages in angiogenic polyps. As previously described, amoeboid microglia/macrophages were frequently found in stage III polyps. Further analysis revealed large cytosolic compartments and tight association of amoeboid microglia/macrophages that occasionally formed clusters and

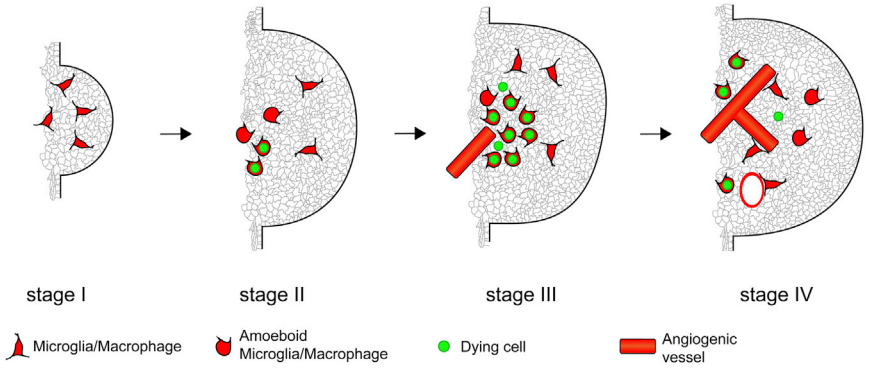

Figure 4. Summary of Microglia/Macrophage Invasion, Cell Death, and Angiogenesis in EGF-Induced Polyps

During the growth of EGF-induced polyps, cell death increases and microglia/macrophages gradually accumulate in the polyp core and adopt an amoeboid morphology (stages I–III). At stage III of polyp development, cell death and microglia/macrophage accumulation reach their peak, and the first signs of angiogenesis are present. As vascularization increases in stage IV polyps, cell death and microglia/macrophage density declines and polyp size increases substantially. Microglia/macrophages associate closely to newly formed vessels and adopt a more ramified morphology.

"string of pearl" structures (Figure 3A). This morphology suggests a common cytosolic syncytium between several microglia/macrophages, similar to what is observed in the development in multinucleated giant cells or cytoplasmic bridges (Evans et al., 1914; Michaels et al., 1988; Hornik et al., 2013).

To study microglia/macrophage ultrastructure in angiogenic and vascularized areas, we utilized transmission electron microscopy. We found cells in the polyp stroma fitting the criteria of amoeboid microglia/macrophages, with an abundance of intracellular vesicles and a rounded cell shape. Moreover, these cells occasionally contained cholesterol crystals and intracellular vesicles (Figure 3B), suggesting phagocytic activity (Tangirala et al., 1994; Klinkner et al., 1995). The phagocytic phenotype suggests a phagosomal and/or lysosomal nature of the intracellular vesicles. Other cells displayed an ultrastructure that inferred a less-activated state, which lacked cholesterol crystals, had a more ramified morphology, and still harbored intracellular vesicles (Figure 3C).

Progressive Cell Death in Developing Polyps, Declining after Angiogenesis

The accumulation and phagocytic activity of microglia/macrophages in the core of the growing polyps could be a consequence of extensive cell death. We used ApopTag labeling to quantify cell death in stage I–IV polyps (Figure 3D). Stage I polyps rarely contained ApopTag$^+$ cells (Figure 3E). In stage II polyps, ApopTag$^+$ cells were occasionally found in the core of the polyps, in areas of IBA1$^+$ cell accumulation (Figure 3F). The density of ApopTag$^+$ cells increased drastically in stage III polyps, concurrent with increasing microglia/macrophage accumulation (Figure 3G). In angiogenic stage IV polyps, prominent cell death was still evident (Figure 3H), albeit at a lower level, compared to stage III polyps.

DISCUSSION

In the current study we demonstrate how EGF infusion leads to polyp development, microglia/macrophage accumulation, and cell death resulting in focal angiogenesis (summarized in Figure 4). Angiogenesis is visible after 14 days of EGF infusion; however, a microglia/macrophage response is present already after 7 days of infusion, preceding angiogenesis. The microglia/macrophage accumulation is concurrent with substantial cell death in the polyp core. Moreover, a significant increase in polyp size is observed when comparing stage III angiogenic polyps to stage IV vascularized polyps, indicating a requirement of angiogenesis for excessive polyp growth.

The delayed response of the SVZ vasculature to grow toward and into the polyps, occurring after more than 7 days of EGF infusion, suggests an indirect mechanism, such as hypoxia, rather than a direct angiogenic effect of EGF infusion. In the cerebral cortex, hypoxia-induced angiogenesis is initiated 7 to 14 days after induction of hypoxia (Masamoto et al., 2013). The accumulation of microglia/macrophages and dying cells in the core of stage III polyps and the subsequent reduction in angiogenic stage IV polyps further strengthens this notion. Whether the microglia/macrophages are attracted by hypoxia-induced signaling or by cell death-related signals remains to be elucidated. However, in the angiogenic stage III polyps, microglia/macrophages adopt an amoeboid morphology, engulf nuclei of dying cells, and display ultrastructural features, suggesting an active role in scavenging dead or dying cells. Microglia and macrophages occasionally express EGFR, and EGF can stimulate microglia migration, acting as a motility factor (Nolte et al., 1997; Planas et al., 1998; Lamb et al., 2004; Qu et al., 2012). However, EGFR expression and chemotactic effects of EGF on microglia/macrophages in vivo appears to be

limited to disease contexts like trauma, neuroinflammation, and atherosclerosis (Lamb et al., 2004; Qu et al., 2012). This could help explain the local, rather than general, microglia/macrophage recruitment after EGF/TGFα infusion, specifically to hyperproliferative areas with extensive cell death in the SVZ demonstrated here and by others (de Chevigny et al., 2008). One possible mechanism behind the microglia/macrophage recruitment could be through production of cytokines like CCL2/MCP-1, TNFα, or IL-1β by microglial cells resident in the growing polyps in response to local hypoxia, like those previously described after hypoxia in the neonatal brain (Deng et al., 2008, 2009). Interestingly, amoeboid microglial cells produce MCP-1 under hypoxia in vitro and express the MCP-1 receptor CCR2 in vivo. When MCP-1 was injected intracerebrally amoeboid microglia cells migrated toward the injection site (Deng et al., 2009). Furthermore, the altered morphology of microglia/macrophages and close association to angiogenic vessels we observe, which occur in stage IV polyps, could represent a change from an angiogenesis-promoting to a vessel-stabilizing role of microglia/macrophages. In the retina, transplanted bone marrow-derived cells differentiate into microglia and promote vessel normalization in a HIF1α-dependent manner (Ritter et al., 2006).

SVZ expansion after EGF treatment is to a large extent caused by extensive proliferation of dysplastic SOX2/OLIG2-expressing cells (Lindberg et al., 2012a). This dysplastic cell type is highly enriched in the polyps and could be involved in microglia/macrophage accumulation and polyp angiogenesis, via paracrine angiogenic signaling. For instance, neural stem cells are known to produce substantial amounts of vascular endothelial growth factor (VEGF) in vitro (Schänzer et al., 2004). Although VEGF does not appear to induce further proliferation of neural stem cells in vitro in the presence of growth factors, neural stem cell-derived VEGF could induce angiogenesis through endothelial cell proliferation (Fabel et al., 2003). The polyps are not only unique in their composition of cells. They lack an ependymal cell layer and the polyps are freely exposed to molecules present in the cerebrospinal fluid (Lindberg et al., 2012a). This could alter the availability of both chemoattractants and angiogenic growth factors in the polyps.

Adult neural stem cells have been suggested as the cells of origin of certain brain tumors (Vescovi et al., 2006). Neural stem cells from animals deficient in *p16* (*Ink4a*) and *p19* (*Arf*) that are retrovirally induced to express constitutively active EGFR persistently form glioma-like tumors in vivo (Bachoo et al., 2002). Moreover, overexpression of wild-type *Egfr* in white matter glial progenitors keeps cells in an immature state, induces extensive migration, and leads to formation of tumor-like white matter hyperplasias (Ivkovic et al., 2008). A small population of stem cell-like cells has been suggested to exist in brain tumors that are treatment resistant and capable of generating secondary tumors (Singh et al., 2004). Much like the supportive niche of neural stem cells, brain tumors appear to modulate the microenvironment to provide conditions promoting stemness (Calabrese et al., 2007). A study investigating human glioblastoma multiforme tumor progression and brain location demonstrated increased risk of multifocal growth and tumor recurrence in tumors located close to the SVZ (Lim et al., 2007). The present study indicates that the SVZ neural stem cell niche can respond to the extensive hyperproliferation by inducing angiogenesis in hyperproliferative areas, possibly supported by microglia/macrophages. Microglia/macrophages in polyps could play a role similar to tumor-associated macrophages, known to contribute to angiogenic processes in tumors (Movahedi et al., 2010; Casazza et al., 2013).

Our results suggest that mechanisms formerly attributed to tumor cells, such as angiogenesis, can be induced in the neurogenic niche. This indicates that some differences between stem cells and tumor cells are context dependent rather than cell intrinsic. Furthermore, our results demonstrate the importance of nonneurogenic cell types in the SVZ niche in the progression of the polyps and their acquired angiogenesis. Whether the observed angiogenesis is more closely related to physiological or pathological angiogenesis remains to be elucidated. Nonetheless, the EGF-infusion model could be useful for increasing our understanding of the events that precede proliferation-related angiogenesis in both health and disease.

EXPERIMENTAL PROCEDURES

Surgery and Tissue Preparation

All experiments were approved by the Gothenburg Committee of the Swedish Animal Welfare Agency (application nos. 214-07 and 145-10). Male Wistar rats (Charles River), 7–8 weeks old, were used in the study. Animals were housed in a barrier facility with ad libitum access to food and water with a 12 hr light/dark cycle. All surgeries were performed under ketamine (33 mg/ml Ketalar, Pfizer) and xylazine (6.67 mg/ml Rompun, Bayer Healthcare AG) anesthesia. The animals were divided into groups receiving either vehicle (aCSF) or EGF (360 ng/day). EGF or vehicle was administered for 7 or 14 days using osmotic minipumps (Model 1002; Alzet-Durect) and infusion cannulas (Brain Infusion Kit 2; Alzet-Durect). The surgeries were performed as previously described (Lindberg et al., 2012a). All animals received three intraperitoneal injections of 50 mg/kg of BrdU during the last 24 hr before perfusion. At the end of the EGF infusion period, animals used for immunofluorescence were sedated using an overdose of pentobarbital and transcardially perfused with sterile 0.9% NaCl followed by phosphate-buffered (0.1 M [pH 7.4]) 4% paraformaldehyde (PFA). Following

perfusion, brains were removed and postfixed in 4% PFA for 24 hr and prepared for cryosectioning by incubation in phosphate-buffered (0.1 M [pH 7.4]) 30% sucrose for at least 3 days. All brains were cryosectioned coronally in 40 μm thick serial sections using a sliding microtome (Leica Microsystems) and collected as serial sections (1 in 12 series with 480 μm distance between sections).

Electron Microscopy

For transmission electron microscopy (TEM), animals were perfused with 0.9% NaCl, followed by 2% PFA and 0.2% glutaraldehyde. The brains were postfixed in 2% PFA and 0.2% glutaraldehyde for 2 hr and stored in 1% PFA at 4°C. The tissue was sectioned at a thickness of 50 μm using a Leica VT1000S vibratome (Leica Microsystems). Tissue was further processed and cut as previously described (Lindberg et al., 2012a). Sections, 60–70 nm thick, were imaged using a LEO912AB transmission electron microscope (Zeiss) equipped with a Megaview III CCD camera (Olympus Soft Imaging Solutions).

Immunohistochemistry

For fluorescent immunohistochemistry, the sections were washed in Tris-buffered saline (TBS). Sections used for BrdU immunofluorescence were treated with 2M HCl for 30 min at 37°C, followed by neutralization in 0.1 M borate buffer. All sections were blocked for 1 hr in TBS with 3% donkey serum and 0.1% Triton-X at room temperature, prior to primary antibody incubation. The following primary antibodies were used: mouse α-rat endothelial cell antigen-1 (RECA-1, 1:300, Monosan), goat α-IBA1 (1:1,000, Abcam), rabbit α-IBA1 (1:1,000, Wako), mouse α-rat CD68 (1:1,000, Millipore), rat α-BrdU (1:500, Serotech), and rabbit α-NG2 (1:500, Millipore). Primary antibody incubation was performed at 4°C for 24–72 hr, followed by washing in TBS. Secondary antibody incubation was performed at room temperature for 2 hr. The following secondary antibodies were used: donkey (dk) α-rabbit IgG CF555, dk α-goat IgG CF555, dk α-goat IgG CF633, dk α-mouse IgG CF488 (Biotium), dk α-rabbit Alexa 488, dk α-goat Alexa 488, and dk α-rat Alexa 488 (Molecular Probes). TOPRO3 was used as nuclear stain (Molecular Probes). After secondary antibody incubation, the sections were washed in TBS and mounted using ProLong Gold with DAPI (Molecular Probes).

Cell Death

For analysis of cell death, ApopTag Fluorescein Direct in situ apoptosis detection kit (Millipore) was used. Sections were mounted on Superfrost Plus microscope slides (Thermo Scientific) and dehydrated in increasing concentrations of ethanol (70–99, 5%), followed by a quick submersion in xylene, rehydration, and wash in TBS. Subsequently, the sections were postfixed in 70% ethanol and acetic acid mixed 2:1 at −20°C for 5 min. To allow proper designation of polyp stage, microglial cells and macrophages were labeled using an Rb α-IBA1 primary antibody (Wako). Following 30 min of blocking, the sections were incubated with the primary antibody for 30 min at 37°C. After washing in TBS sections were incubated with a dk α-rabbit Alexa 555 secondary antibody and TOPRO3 nuclear dye for 30 min at 37°C, followed by washing. Dying cells were labeled in accordance with the manufacturer's instructions.

Confocal Microscopy and Quantification

Immunofluorescence was visualized using a Leica SP2 (Leica Microsystems) and a Zeiss LSM 710 (Carl Zeiss) inverted confocal microscope. The image stacks were processed in ImageJ (http://rsbweb.nih.gov/ij/) and arranged in Adobe Photoshop CS5 and Adobe Illustrator CS5 (Adobe Systems). When studying double labeling, image stacks were acquired at 0.5 μm increments, and orthogonal views were used to determine colocalization and double labeling in single cells. Images used for quantification of polyp size, IBA1$^+$ cell density, and IBA1/CD68 coexpression, and ApopTag labeling was quantified in ImageJ using the LOCI plugin.

Statistics

All statistical analysis was performed in Prism 6 (Graphpad Software). Means in polyp size comparing 7 and 14 days are presented with standard deviation and compared using a two-tailed Student's t test. For statistical analysis comparing more than two groups, a one-way ANOVA was used, in conjunction with Tukey's post-hoc test and presented as means ± SEM. Differences in means resulting in values of $p < 0.05$ were considered statistically significant.

ACKNOWLEDGMENTS

The authors would like to thank Birgit Linder and Ann-Marie Alborn for excellent technical assistance and the Center for Cellular Imaging and the Electron Microscopy Unit at Gothenburg University for their technical support. The authors would also like to thank Ahmed Osman for help with the ApopTag assay. This work was supported by grants from the Swedish Medical Research Council (http://www.vr.se), Västra Götaland regional funds for biomedical research (LUA-ALF), the Swedish Childhood Cancer Foundation, the Swedish Brain Foundation, Stroke-Riksförbundet, Rune och Ulla Amlövs stiftelse, Stiftelsen Edit Jacobssons donationsfond, and Stiftelsen Wilhelm och Martina Lundgrens Vetenskapsfond.

Received: November 30, 2013
Revised: February 11, 2014
Accepted: February 12, 2014
Published: March 27, 2014

REFERENCES

Altman, J. (1969). Autoradiographic and histological studies of postnatal neurogenesis. IV. Cell proliferation and migration in the anterior forebrain, with special reference to persisting neurogenesis in the olfactory bulb. J. Comp. Neurol. *137*, 433–457.

Arnold, T., and Betsholtz, C. (2013). The importance of microglia in the development of the vasculature in the central nervous system. Vasc. Cell *5*, 4.

Bachoo, R.M., Maher, E.A., Ligon, K.L., Sharpless, N.E., Chan, S.S., You, M.J., Tang, Y., DeFrances, J., Stover, E., Weissleder, R., et al. (2002). Epidermal growth factor receptor and Ink4a/Arf: convergent mechanisms governing terminal differentiation and

transformation along the neural stem cell to astrocyte axis. Cancer Cell *1*, 269–277.

Bourghardt Peebo, B., Fagerholm, P., Traneus-Röckert, C., and Lagali, N. (2011). Time-lapse in vivo imaging of corneal angiogenesis: the role of inflammatory cells in capillary sprouting. Invest. Ophthalmol. Vis. Sci. *52*, 3060–3068.

Bovetti, S., Hsieh, Y.C., Bovolin, P., Perroteau, I., Kazunori, T., and Puche, A.C. (2007). Blood vessels form a scaffold for neuroblast migration in the adult olfactory bulb. J. Neurosci. *27*, 5976–5980.

Calabrese, C., Poppleton, H., Kocak, M., Hogg, T.L., Fuller, C., Hamner, B., Oh, E.Y., Gaber, M.W., Finklestein, D., Allen, M., et al. (2007). A perivascular niche for brain tumor stem cells. Cancer Cell *11*, 69–82.

Casazza, A., Laoui, D., Wenes, M., Rizzolio, S., Bassani, N., Mambretti, M., Deschoemaeker, S., Van Ginderachter, J.A., Tamagnone, L., and Mazzone, M. (2013). Impeding macrophage entry into hypoxic tumor areas by Sema3A/Nrp1 signaling blockade inhibits angiogenesis and restores antitumor immunity. Cancer Cell *24*, 695–709.

Checchin, D., Sennlaub, F., Levavasseur, E., Leduc, M., and Chemtob, S. (2006). Potential role of microglia in retinal blood vessel formation. Invest. Ophthalmol. Vis. Sci. *47*, 3595–3602.

Craig, C.G., Tropepe, V., Morshead, C.M., Reynolds, B.A., Weiss, S., and van der Kooy, D. (1996). In vivo growth factor expansion of endogenous subependymal neural precursor cell populations in the adult mouse brain. J. Neurosci. *16*, 2649–2658.

de Chevigny, A., Cooper, O., Vinuela, A., Reske-Nielsen, C., Lagace, D.C., Eisch, A.J., and Isacson, O. (2008). Fate mapping and lineage analyses demonstrate the production of a large number of striatal neuroblasts after transforming growth factor alpha and noggin striatal infusions into the dopamine-depleted striatum. Stem Cells *26*, 2349–2360.

Deng, Y., Lu, J., Sivakumar, V., Ling, E.A., and Kaur, C. (2008). Amoeboid microglia in the periventricular white matter induce oligodendrocyte damage through expression of proinflammatory cytokines via MAP kinase signaling pathway in hypoxic neonatal rats. Brain Pathol. *18*, 387–400.

Deng, Y.Y., Lu, J., Ling, E.A., and Kaur, C. (2009). Monocyte chemoattractant protein-1 (MCP-1) produced via NF-kappaB signaling pathway mediates migration of amoeboid microglia in the periventricular white matter in hypoxic neonatal rats. Glia *57*, 604–621.

Doetsch, F., García-Verdugo, J.M., and Alvarez-Buylla, A. (1997). Cellular composition and three-dimensional organization of the subventricular germinal zone in the adult mammalian brain. J. Neurosci. *17*, 5046–5061.

Doetsch, F., Petreanu, L., Caille, I., Garcia-Verdugo, J.M., and Alvarez-Buylla, A. (2002). EGF converts transit-amplifying neurogenic precursors in the adult brain into multipotent stem cells. Neuron *36*, 1021–1034.

Evans, H.M., Bowman, F.B., and Winternitz, M.C. (1914). An experimental study of the histogenesis of the miliary tubercle in vitally stained rabbits. J. Exp. Med. *19*, 283–302.

Fabel, K., Fabel, K., Tam, B., Kaufer, D., Baiker, A., Simmons, N., Kuo, C.J., and Palmer, T.D. (2003). VEGF is necessary for exercise-induced adult hippocampal neurogenesis. Eur. J. Neurosci. *18*, 2803–2812.

Gonzalez-Perez, O., Romero-Rodriguez, R., Soriano-Navarro, M., Garcia-Verdugo, J.M., and Alvarez-Buylla, A. (2009). Epidermal growth factor induces the progeny of subventricular zone type B cells to migrate and differentiate into oligodendrocytes. Stem Cells *27*, 2032–2043.

Hornik, T.C., Neniskyte, U., and Brown, G.C. (2013). Inflammation induces multinucleation of microglia via PKC inhibition of cytokinesis, generating highly phagocytic multinucleated giant cells. J. Neurochem. http://dx.doi.org/10.1111/jnc.12477.

Ivkovic, S., Canoll, P., and Goldman, J.E. (2008). Constitutive EGFR signaling in oligodendrocyte progenitors leads to diffuse hyperplasia in postnatal white matter. J. Neurosci. *28*, 914–922.

Kettenmann, H., Hanisch, U.K., Noda, M., and Verkhratsky, A. (2011). Physiology of microglia. Physiol. Rev. *91*, 461–553.

Klinkner, A.M., Waites, C.R., Kerns, W.D., and Bugelski, P.J. (1995). Evidence of foam cell and cholesterol crystal formation in macrophages incubated with oxidized LDL by fluorescence and electron microscopy. J. Histochem. Cytochem. *43*, 1071–1078.

Kokovay, E., Goderie, S., Wang, Y., Lotz, S., Lin, G., Sun, Y., Roysam, B., Shen, Q., and Temple, S. (2010). Adult SVZ lineage cells home to and leave the vascular niche via differential responses to SDF1/CXCR4 signaling. Cell Stem Cell *7*, 163–173.

Kuhn, H.G., Winkler, J., Kempermann, G., Thal, L.J., and Gage, F.H. (1997). Epidermal growth factor and fibroblast growth factor-2 have different effects on neural progenitors in the adult rat brain. J. Neurosci. *17*, 5820–5829.

Lamb, D.J., Modjtahedi, H., Plant, N.J., and Ferns, G.A. (2004). EGF mediates monocyte chemotaxis and macrophage proliferation and EGF receptor is expressed in atherosclerotic plaques. Atherosclerosis *176*, 21–26.

Liao, H., Huang, W., Niu, R., Sun, L., and Zhang, L. (2008). Cross-talk between the epidermal growth factor-like repeats/fibronectin 6-8 repeats domains of Tenascin-R and microglia modulates neural stem/progenitor cell proliferation and differentiation. J. Neurosci. Res. *86*, 27–34.

Lim, D.A., Cha, S., Mayo, M.C., Chen, M.H., Keles, E., VandenBerg, S., and Berger, M.S. (2007). Relationship of glioblastoma multiforme to neural stem cell regions predicts invasive and multifocal tumor phenotype. Neuro-oncol. *9*, 424–429.

Lindberg, O.R., Brederlau, A., Jansson, A., Nannmark, U., Cooper-Kuhn, C., and Kuhn, H.G. (2012a). Characterization of epidermal growth factor-induced dysplasia in the adult rat subventricular zone. Stem Cells Dev. *21*, 1356–1366.

Lindberg, O.R., Persson, A., Brederlau, A., Shabro, A., and Kuhn, H.G. (2012b). EGF-induced expansion of migratory cells in the rostral migratory stream. PLoS ONE *7*, e46380.

Luskin, M.B. (1993). Restricted proliferation and migration of postnatally generated neurons derived from the forebrain subventricular zone. Neuron *11*, 173–189.

Masamoto, K., Takuwa, H., Tomita, Y., Toriumi, H., Unekawa, M., Taniguchi, J., Kawaguchi, H., Itoh, Y., Suzuki, N., Ito, H., and Kanno, I. (2013). Hypoxia-induced cerebral angiogenesis in

mouse cortex with two-photon microscopy. Adv. Exp. Med. Biol. *789*, 15–20.

Michaels, J., Price, R.W., and Rosenblum, M.K. (1988). Microglia in the giant cell encephalitis of acquired immune deficiency syndrome: proliferation, infection and fusion. Acta Neuropathol. *76*, 373–379.

Mirzadeh, Z., Merkle, F.T., Soriano-Navarro, M., Garcia-Verdugo, J.M., and Alvarez-Buylla, A. (2008). Neural stem cells confer unique pinwheel architecture to the ventricular surface in neurogenic regions of the adult brain. Cell Stem Cell *3*, 265–278.

Movahedi, K., Laoui, D., Gysemans, C., Baeten, M., Stangé, G., Van den Bossche, J., Mack, M., Pipeleers, D., In't Veld, P., De Baetselier, P., and Van Ginderachter, J.A. (2010). Different tumor microenvironments contain functionally distinct subsets of macrophages derived from Ly6C(high) monocytes. Cancer Res. *70*, 5728–5739.

Nolte, C., Kirchhoff, F., and Kettenmann, H. (1997). Epidermal growth factor is a motility factor for microglial cells in vitro: evidence for EGF receptor expression. Eur. J. Neurosci. *9*, 1690–1698.

Planas, A.M., Justicia, C., Soriano, M.A., and Ferrer, I. (1998). Epidermal growth factor receptor in proliferating reactive glia following transient focal ischemia in the rat brain. Glia *23*, 120–129.

Qu, W.S., Tian, D.S., Guo, Z.B., Fang, J., Zhang, Q., Yu, Z.Y., Xie, M.J., Zhang, H.Q., Lü, J.G., and Wang, W. (2012). Inhibition of EGFR/MAPK signaling reduces microglial inflammatory response and the associated secondary damage in rats after spinal cord injury. J. Neuroinflammation *9*, 178.

Ritter, M.R., Banin, E., Moreno, S.K., Aguilar, E., Dorrell, M.I., and Friedlander, M. (2006). Myeloid progenitors differentiate into microglia and promote vascular repair in a model of ischemic retinopathy. J. Clin. Invest. *116*, 3266–3276.

Schänzer, A., Wachs, F.P., Wilhelm, D., Acker, T., Cooper-Kuhn, C., Beck, H., Winkler, J., Aigner, L., Plate, K.H., and Kuhn, H.G. (2004). Direct stimulation of adult neural stem cells in vitro and neurogenesis in vivo by vascular endothelial growth factor. Brain Pathol. *14*, 237–248.

Shen, Q., Wang, Y., Kokovay, E., Lin, G., Chuang, S.M., Goderie, S.K., Roysam, B., and Temple, S. (2008). Adult SVZ stem cells lie in a vascular niche: a quantitative analysis of niche cell-cell interactions. Cell Stem Cell *3*, 289–300.

Singh, S.K., Hawkins, C., Clarke, I.D., Squire, J.A., Bayani, J., Hide, T., Henkelman, R.M., Cusimano, M.D., and Dirks, P.B. (2004). Identification of human brain tumour initiating cells. Nature *432*, 396–401.

Tangirala, R.K., Jerome, W.G., Jones, N.L., Small, D.M., Johnson, W.J., Glick, J.M., Mahlberg, F.H., and Rothblat, G.H. (1994). Formation of cholesterol monohydrate crystals in macrophage-derived foam cells. J. Lipid Res. *35*, 93–104.

Tavazoie, M., Van der Veken, L., Silva-Vargas, V., Louissaint, M., Colonna, L., Zaidi, B., Garcia-Verdugo, J.M., and Doetsch, F. (2008). A specialized vascular niche for adult neural stem cells. Cell Stem Cell *3*, 279–288.

Unoki, N., Murakami, T., Nishijima, K., Ogino, K., van Rooijen, N., and Yoshimura, N. (2010). SDF-1/CXCR4 contributes to the activation of tip cells and microglia in retinal angiogenesis. Invest. Ophthalmol. Vis. Sci. *51*, 3362–3371.

Vescovi, A.L., Galli, R., and Reynolds, B.A. (2006). Brain tumour stem cells. Nat. Rev. Cancer *6*, 425–436.

Walton, N.M., Sutter, B.M., Laywell, E.D., Levkoff, L.H., Kearns, S.M., Marshall, G.P., 2nd, Scheffler, B., and Steindler, D.A. (2006). Microglia instruct subventricular zone neurogenesis. Glia *54*, 815–825.